NANO LETTERS

Letter

pubs.acs.org/NanoLett

Atomic Defects Influenced Mechanics of II–VI Nanocrystals

Moumita Ghosh,[*,†,‡,¶] Siddharth Ghosh,[*,§] Hamed Attariani,[∥] Kasra Momeni,[*,⊥,#] Michael Seibt,[¶] and Gowravaram Mohan Rao[‡]

[†]Centre for Nano Science and Engineering, Indian Institute of Science, Bangalore, 560012 Karnataka, India

[‡]Department of Instrumentation and Applied Physics, Indian Institute of Science, Bangalore, 560012 Karnataka, India

[¶]IV[th] Institute of Physics - Solids and Nanostructures, Georg-August-Universität-Göttingen, Friedrich-Hund-Platz 1, Göttingen 37077, Germany

[§]III[rd] Institute of Physics - Biophysics and Complex Systems, Georg-August-Universität-Göttingen, Friedrich-Hund-Platz 1, Göttingen 37077, Germany

[∥]Department of Mechanical Engineering, Wright State University, Dayton, Ohio 45435, United States

[⊥]Department of Materials Science and Engineering, Pennsylvania State University, State College, Pennsylvania 16802, United States

[#]Department of Materials Science and Engineering, Louisiana Tech University, Ruston, Louisiana 16802, United States

Supporting Information

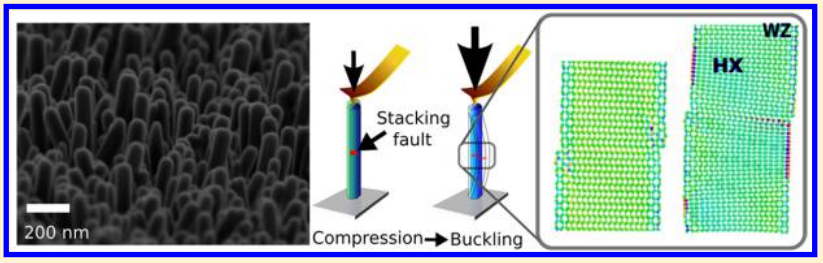

ABSTRACT: Mechanical properties of nanocrystals are influenced by atomic defects. Here, we demonstrate the effect of planar defects on the mechanics of ZnO nanorods using atomic force microscopy, high-resolution transmission electron microscopy, and large-scale atomistic simulation. We study two different conditionally grown single nanorods. One contains extended I_1-type stacking fault (SF) and another is defect free. The SF containing nanorods show buckling behaviors with reduced critical loading, whereas the other kinds show linear elastic behavior. We also studied the size dependence of elastic modulus and yield strength. The elastic modulus in both nanorods is inversely proportional to their size. Similar trend is observed for yield strength in the SF containing nanorods; however, the opposite is observed in the SF-free nanorods. This first experimental and theoretical study will guide toward the development of reliable electromechanical devices.

KEYWORDS: *Zinc oxide nanorods, atomic defects, mechanical properties, phase transformation, molecular dynamics, atomic force microscopy*

Electromechanics is one of the prominent fields of research today due to its wide application from energy harvesting[1] to nanoscale biomanipulation through actuation.[2] The active materials of electromechanical devices are being aimed for piezoelectric nanostructures to obtain high electrical energy conversion efficiency and power density. Significant number of studies are conducted on these nanostructures of different materials. Among them, one of the environmentally friendly, extensively studied nanomaterials is of II–VI groups such as zinc oxide (ZnO).[3−7] At nanometer scale, the wurtzite ZnO nanorods are shown to be single crystalline with the highest piezoelectric response among the tetrahedrally bonded semiconductors.[8−10] Furthermore, the nanorods are more flexible[11] and have higher elastic modulus[12,13] and piezoelectric coefficient[14−16] than the bulk ZnO.

With the rapidly growing number of studies on the electromechanical behavior of ZnO nanostructures in the fields of nanogenerators[17] and nanopiezoelectronics,[18] investigation of its mechanical behavior is important. Previously, several investigations using different experimental methods showed anomaly in the measured elastic modulus of ZnO nanostructures[19−23] compared to the bulk ZnO. Elastic modulus is an intensive property of a material, independent of shape and geometry of a material, whereas the aforementioned investigated elastic moduli are extensively property-dependent such as geometry, shape, and boundary condition. So, they can not be called true elastic moduli of ZnO. However, theoretical estimations of ZnO nanorods without any structural defects show that with reducing diameter the elastic modulus of 1D ZnO nanostructures increases.[11,12,24,25] Despite the importance

Received: February 9, 2016
Revised: August 23, 2016

DOI: 10.1021/acs.nanolett.6b00571
Nano Lett. XXXX, XXX, XXX−XXX

of defects in determining the final strength of materials, there is only a limited number of studies on 1D ZnO nanostructures,[26] which show reduction in fracture strength due to presence of voids that ultimately change the piezoelectric response of ZnO nanostructures.[14,27]

Here, we provide a new insight into the mechanical property degradation of undoped ZnO nanorods and its relation with atomic defects, such as stacking faults (SFs) using atomic force microscopy (AFM), high-resolution transmission electron microscopy (HRTEM), and scanning electron microscopy (SEM) on two different ZnO nanorod specimens with similar morphology but different growth conditions. We also performed large-scale molecular dynamics (MD) simulations on two different types of ZnO nanorods (SF free and with SF) to correlate our experimental observations from AFM and HRTEM. The morphology of undoped, vertically aligned [0001] ZnO nanorods grown at 95 °C[15] with diameters 50−60 nm is shown in Figure 1a, as observed from the SEM. Similar growth morphology with nearly the same diameter (50−70 nm) is observed at 85 °C. Details of growth and morphology of the 85 °C grown ZnO nanorods, which are SF free, are given in Figure S1a. Mechanical stability of these two types of ZnO nanorods were studied using AFM indentation. The [0001] ZnO nanorods are polar at the top and bottom *c*-planes, and application of force along the [0001] direction generates higher electric charge[28] across the two poles than the other directions of the nanorods. Therefore, for mechanical stability analysis we applied vertical force parallel to the [0001] direction of these nanorods through an AFM tip (Figure S2) and measured the maximum possible vertical force applicable without structural failure. The cross-sectional SEM images (Figure S1b) of these nanorods show that their bases are not agglomerated. We observed similar cross-sectional view for both types of nanorod samples. This avoids the possibility of measuring ensemble or coupled mechanics of several nanorods. Further, it is also important to make sure that the force is applied vertically on the nanorods as inclination of the nanorods can lead to erroneous measurements. From the SEM images, it is evident that all the nanorods are not strictly perpendicular to the substrate. We utilized AFM profiling of the nanorods (Figure S5a−c) to differentiate vertically aligned and inclined nanorods. The characteristic difference of the scan profile is dependent on the angular distribution of the nanorods as well as on the dilation effect of the AFM probe. A vertically aligned nanorod always produces isotropic Gaussian profile distribution, while an inclined nanorod produces a Poissonian profile. This characteristic behavior of the profile enables us to distinguish the vertically aligned ZnO nanorods from the inclined nanorods. Here, we indented only on the vertically aligned ZnO nanorods using their distinctive scan profiles. In Figure 1b,c, we show AFM force−displacement (FD) curves of two single ZnO nanorods grown at 85 and 95 °C, respectively. The AFM tapping mode topography of these ZnO nanorods are shown in the respective insets. In both the cases, the FD curves are obtained from DZ (tip deflection error vs piezo displacement) curves as shown in the insets. They were measured at the black crossed regions in the corresponding topographies (due to the AFM tip dilation effect ZnO nanorods appear to be nonhexagonal). The elastic modulus (Y_{exp}) was quantified by fitting the Sneddon model to the FD retraction curve. Justification of using Sneddon model is detailed in the Supporting Information, section 4. A 85 °C grown nanorod shows Y_{exp} as 145 GPa upon relaxing a vertical compressive force within the linear elastic domain along the [0001] direction (illustrated in the inset). The nanorods chosen in Figure 1 have a minimum separation distance of 10 nm from their neighboring nanorods, which is sufficient to prevent interference in the measurements from the neighboring nanorods. We carried out 11 measurements on different nanorods of the same sample where the Y_{exp} was ranged from 129 to 145 GPa. It is close to the previously reported bulk elastic modulus (140 GPa) of ZnO in the [0001] direction.[12,24,25] Later, we also investigate this in an MD simulation framework. On the contrary, the nanorod grown at 95 °C (Figure 1a) shows a sudden change in slope of the FD approach curve at 78 nN under compressive loading (Figure 1c). We consider this as a critical force (F_{cr}). In the retraction curve we also observe another kink close to F_{cr} at 84 nN. These indicate a typical buckling behavior of the nanorod.[29] This sudden change in the slope is also noticed in the DZ curve (as shown in the inset). The schematic of the buckling event is depicted in the Figure 1c. Repeated FD curve measurements at different places of the same sample show similar buckling behavior with low value of F_{cr} from 20 to 80 nN (Figure S6a). Later, we discuss about the reasoning behind such low F_{cr} after understanding the atomistic scenario using MD simulations.

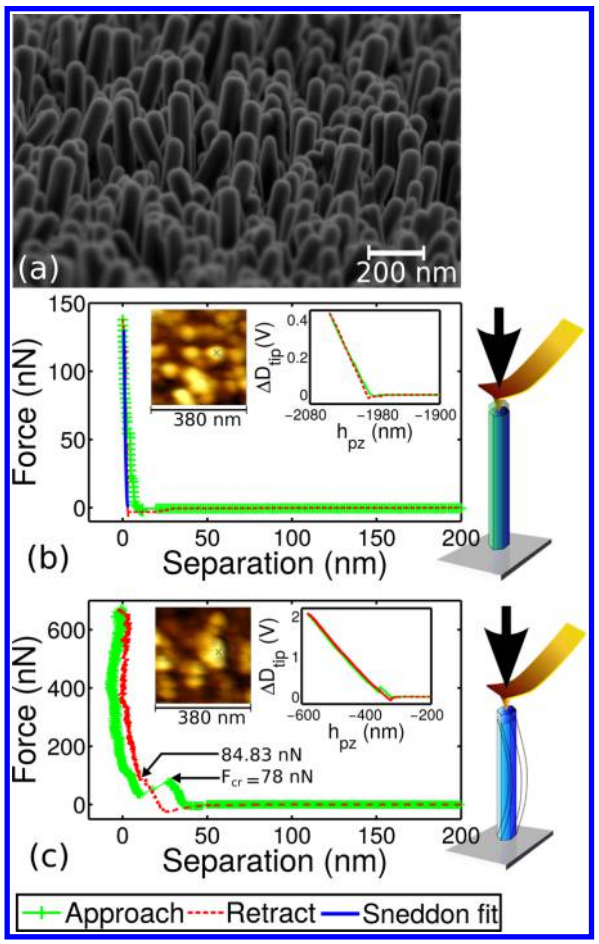

Figure 1. (a) SEM image of vertically aligned ZnO nanorods. (b,c) FD curves of ZnO nanorods grown at 85 and 95 °C, respectively. Insets show indentation region on AFM topography, the corresponding DZ curves, and the schematics of AFM tip-nanorod interaction. In the AFM topography, the nanorods appear to be nondiscrete due to the dilation effect of the AFM tip.

DOI: 10.1021/acs.nanolett.6b00571
Nano Lett. XXXX, XXX, XXX−XXX

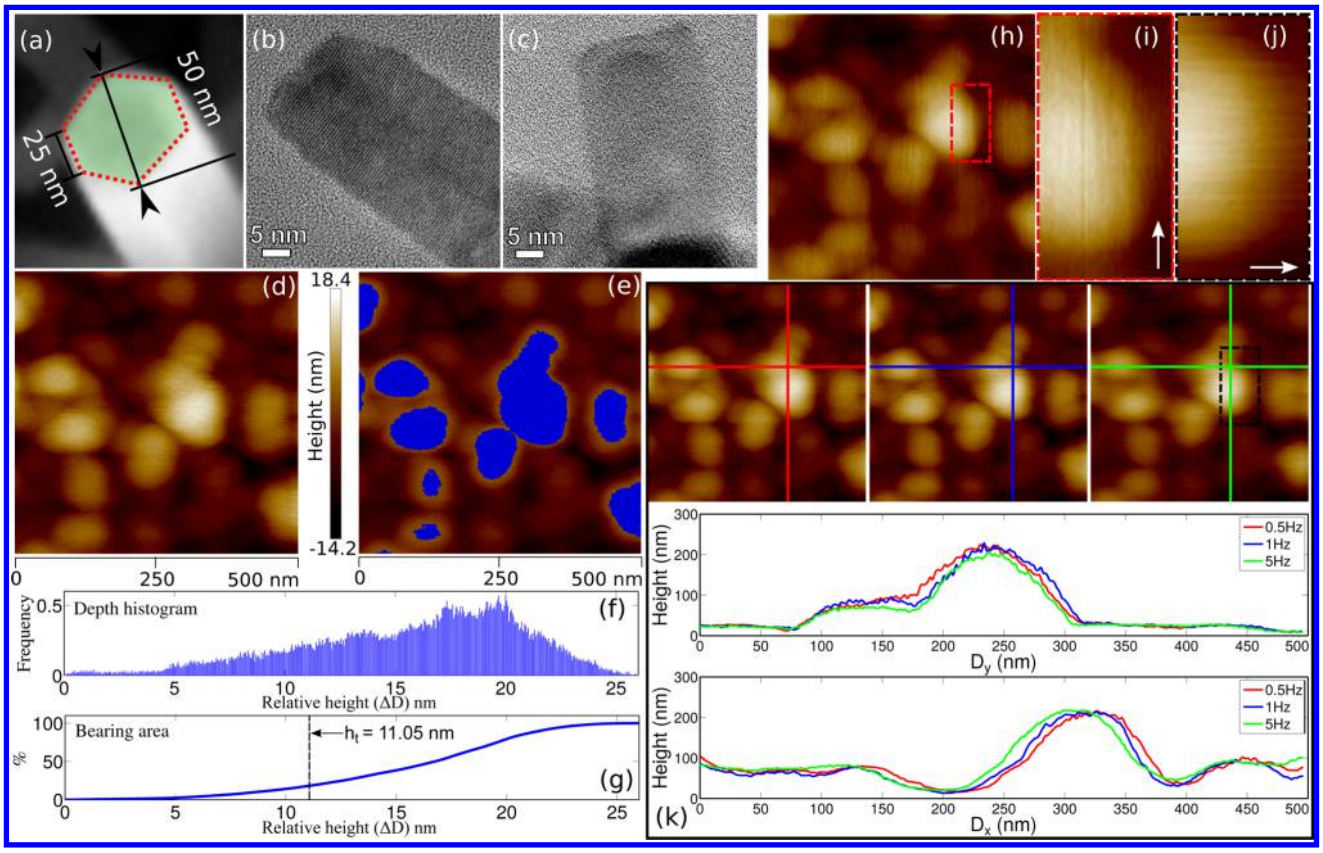

Figure 2. (a) SEM tilted view of a hexagonal ZnO nanorod specimen of width 50 nm grown at 95 °C. (b,c) HRTEM of ZnO nanorods taken from the same sample. (d,e) AFM topographic image of height threshold (h_t) specific density mapping of nanorods (blue encoded region > h_t = 11.05 nm), (f) depth histogram, and (g) bearing area analysis. (h) A 90° rotated scanned view of the same area as shown in figure (d). (i,j) Magnified view of these images with y and x scan directions, respectively. (k) Drift in position of the nanorods with different scan speeds from 0.5 to 5 Hz (left to right) with plots showing vertical and horizontal scans, respectively.

Buckling sometimes leads to slip-induced interaction with the neighbor nanorods. The FD behavior of such interaction is detailed in Figure S5d–f. Although not all the nanorods grown on the substrate are perpendicular (with maximum ±10° tilt) to the substrate, we followed the procedure described in Figure S5 to choose nanorods that are grown normal to the substrate to ensure the correctness of the measurements.

A crucial part of these measurements is to avoid slip of the cantilever tip from the top surface of the nanorods. We used a position mapping protocol to ensure that the point of contact of the applied force is precisely on top of a single ∼50 nm wide ZnO nanorod (Figure 2a). The SEM and HRTEM images, shown in Figure 2a–c, show hexagonal and flat top surface of these nanorods. During the FD curve measurements, at first we obtained the topography of a 500 × 500 nm^2 area of the ZnO nanorods by tapping mode as shown in Figure 2d. In Figure 2e, we compute a height threshold (h_t) specific density mapping of the nanorods, where the blue encoded pixels denote height greater than h_t (= 11.05 nm here). In the depth histogram (Figure 2f) of the relative height (Δh), we observe several peaks after 11.05 nm (i.e., many of the nanorods are taller than this height) justifying the choice of 11.05 nm as h_t. The highest peak observed in the histogram is at 20 nm, which infers majority of the nanorods have $\Delta h > h_t$. We also analyzed the percentage of bearing area in Figure 2g, where majority of the pixels are above h_t and 20% are below. These indicate the height homogeneity of the ZnO nanorods in the sample at certain depth. To avoid imaging artifacts, we rescanned the same area of Figure 2d by rotating 90°. The corresponding 90° rotated view is shown in Figure 2h. Similar topographies in both the images confirm presence of ZnO nanorods instead of any artifact. Figure 2i,j shows magnified view of a nanorod using horizontal and vertical scans, where the arrows indicate the scan directions. We also quantify presence of mechanical drift by imaging them at different scan frequencies (0.5 to 5 Hz, Figure 2k). We observe total drift of 18 and 7 nm in horizontal (D_x) and vertical (D_y) axes, respectively. At 5 and 0.5 Hz scan frequencies we observe large drift and drag effect, respectively. Therefore, it was unreliable to measure FD on the topographies scanned using both the frequencies. At scan speed 1 Hz, we observed low drift (D_x = 8 nm, D_y = 4 nm) and drag in the AFM images. So, we chose 1 Hz to map the topography of a small area on the same sample and then apply vertical force through the cantilever tip on a single ZnO nanorod. This procedure was followed for both types of ZnO nanorods, but here in Figure 2, we demonstrated this with the 95 °C grown nanorods.

We carried out a series of analytical calculations in the Supporting Information by considering experimental conditions, such as F_{cr} and boundary conditions (Figure S6b,d). A similar approach was realized earlier.[21] However, these results are inconclusive as they are dependent on variable boundary conditions and geometry of the structures. To understand the discrepancy in the measured mechanical properties between two types of ZnO nanorods with similar morphology, we further investigate the 95 °C grown nanorods under HRTEM.

DOI: 10.1021/acs.nanolett.6b00571
Nano Lett. XXXX, XXX, XXX−XXX

During HRTEM measurements the incident electron beam was along the [110] direction (Figure 3a) of the ZnO nanorod; the

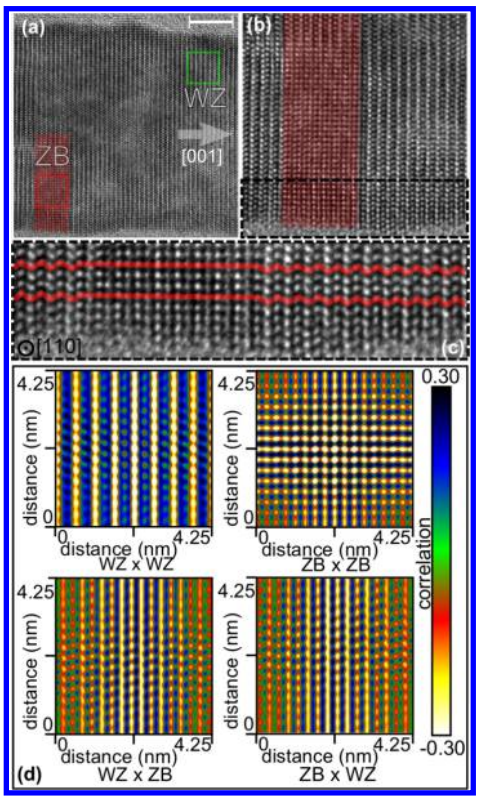

Figure 3. (a–c) HRTEM of ZnO nanorod (scale bar 5 nm) showing extended I_1-type SF in the enlarged view, where the wurtzite stacking (abab...) is changed into zinc blend (abc..), which is continued for 4.25 nm. Here, incident electron beam direction is along the [110]. (d) Autocorrelation (WZ × WZ and ZB × ZB) and cross-correlation (WZ × ZB and ZB × WZ) of SF free (WZ, green box from (a)) and SF containing (ZB, red box from (a)) regions, respectively. The cross-correlations has no similarities with the autocorrelations, which is a quantitative evidence of presence of ZB-based stacking fault.

corresponding electron diffractogram is shown in Figure S8. The electron diffractogram confirms the [0001] growth direction and wurtzite phase of the ZnO nanorod. A magnified view of the red highlighted area of Figure 3a is shown in Figure 3b, which shows a basal plane SF in the nanorod. A portion of this area is further magnified in Figure 3c for defect analysis. Here, the red lines clearly show discontinuity in the wurtzite (WZ) stacking and presence of zincblende (ZB) stacking (Figure S9) in the ZnO nanorod. This type of planar defect is an I_1-type extended SF.[30,31] For quantitative defect analysis, we perform correlation studies between an SF-free (green square region, WZ, Figure 3a) and SF containing region (red square region, ZB, Figure 3a). These show that the cross-correlation (WZ × ZB and ZB × WZ) images are substantially different from the autocorrelations (WZ × WZ and ZB × ZB).

To realize the effect of SF on mechanical properties of the wurtzite ZnO nanorods, we performed classical MD simulations on wurtzite ZnO nanorods of infinite length with periodic boundary condition along the [0001] direction. We considered an SF as mentioned in the Supporting Information, section 10. The designated coordinate system, the crystal structure, and the growth direction of the ZnO nanorods were considered for simulations are shown in Figure 4a–c. From the

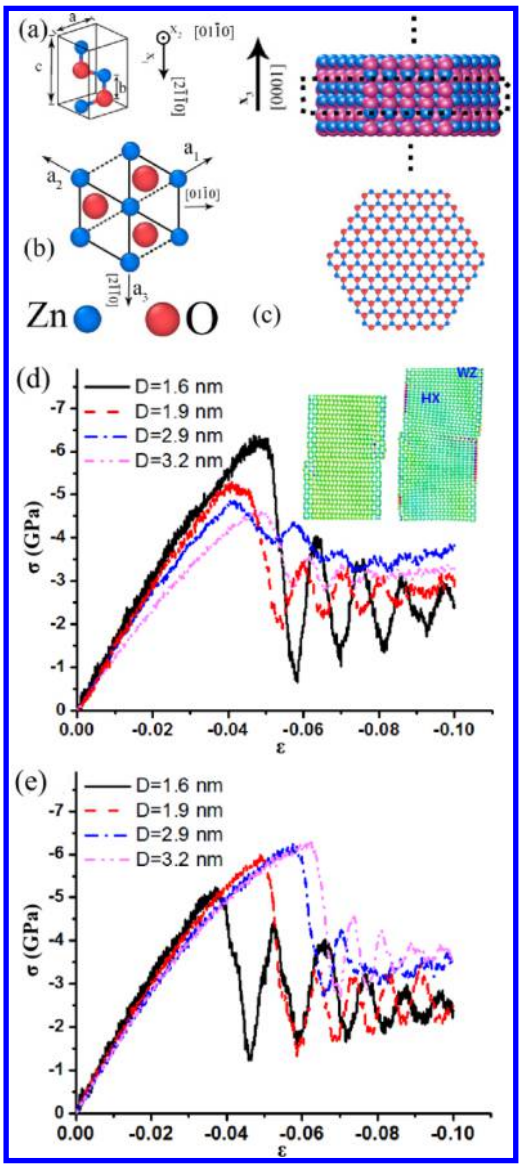

Figure 4. Crystal structure and geometry of 1D ZnO nanostructures along with mechanical response and phase transformations. (a) Unit cell of the wurtzite ZnO crystal structure with a lattice constant a in the basal plane, c is the unit vector along [0001], and b is the nearest-neighbor distance; (b) top view of the crystal structure of hexagonal wurtzite normal to [0001]; and (c) side view and top view of a ZnO nanorod grown along c-axis. The SF is enclosed within a dotted box. The utilized Cartesian coordinate system, x_i, is shown along the specified crystal directions. (d,e) The (virial) stress vs strain curves for ZnO nanorods of diameter 1.6–3.2 nm with SF and without SF, respectively, under uniaxial compressive loadings. During compression WZ to HX phase transformation for nanorods starts from one side of the SF and propagates laterally (inset figure).

simulations, the (virial) stress–strain curves[32] are plotted (Figure 4d,e) for nanorods (with a single I_1-type SF as well as for nanorods without SF) with different diameters, and the compressive elastic modulus (Y_{MD}) and yield strength (σ_y, at which the ZnO nanorod deforms plastically) are also extracted. The MD simulations indicate a different phase transformation kinetics in the presence of an SF. The abrupt change in the stress–strain curve illustrates wurtzite to hexagonal (HX) phase transformation. Under compressive loading, this phase transformation initiates from the surface at the compressive side of

DOI: 10.1021/acs.nanolett.6b00571
Nano Lett. XXXX, XXX, XXX–XXX

the SF, which causes a bending stress and further phase transformation to HX on the other side of the nanorod. The phase transformation extends radially and along the axis of the nanorod. Until the nanorod completely transforms into HX followed by an elastic loading, delayed phase transformation occurs on the side of the SF where atoms are under tensile stress. So, the phase transformation of ZnO nanorods under uniaxial compression starts from the SF and propagates throughout the entire nanorod at the yield stress (inset in Figure 4d) as the compressive force increases. It is worth noting that the stress-relaxation in such ZnO nanorod occurs through phase transformation that is a different mechanism from what is reported in nanorods with a FCC crystal structure, i.e., nucleation and transformation of dislocations.[33]

We observed variation in Y_{MD} of the nanorod as a function of diameter as shown in Figure 5a. It indicates an enhancement of

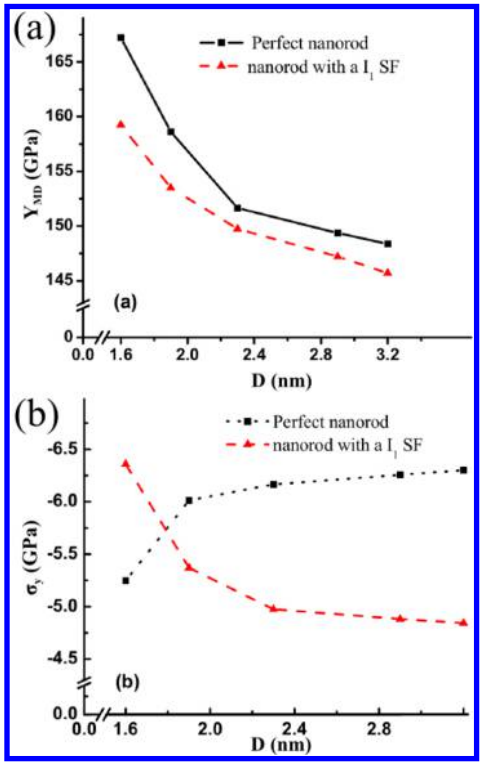

Figure 5. (a) Elastic modulus (Y_{MD}) reduces as a function of diameter, and nanorods with a single SF have lower elastic modulus compared to an SF free nanorod. (b) Yield strength (σ_y) increases by increasing the diameter for SF free perfect nanorods, while it has an inverse trend for the nanorods with a single SF.

Y_{MD} while decreasing the diameter. This happens due to surface-relaxation where the external surface is under compression, while the inner atomic layers are stretched due to long-range electrostatic interactions. Contraction of surface atoms results in reduction of interatomic distances. A subsequent increase in the Y_{MD} of surface-layer atoms is given by $Y_{MD} \propto d^{-4}$, where d is the interatomic distance.[34] Here, the Y_{MD} decreases as the diameter increases because surface energy contribution reduces more rapidly compared to the bulk energy. The σ_y as a function of diameter shown in Figure 5b demonstrates the same trend as the Y_{MD} for the nanorod with SF. However, an inverse trend for the SF free perfect nanorod is observed where it reaches a plateau when the diameter is greater than 3.2 nm. The σ_y is greater for a nanorod of diameter 1.6 nm with an SF compared to an SF free nanorod by ~21%. There is a turnover in the σ_y of nanorod with a single SF defect at the 1.8 nm diameter, where an SF free nanorod has a greater σ_y. The results show strain-rate ($\dot{\epsilon}$) independence over the range of $10^{12}\ s^{-1} \leq \dot{\epsilon} \leq 6 \times 10^{12}\ s^{-1}$; and no strain-rate amorphization was observed in this range. These atomic simulations show significant surface relaxation of the first two outermost layers of atoms in the nanorod where the core-atoms undergo relaxation due to long-range electrostatic interactions to satisfy the stress-free boundary conditions. Moreover, the atomic reconstruction is also revealed at the intersection of SF and external surface. Here, compressive stresses, which are revealed on one side of SF, are compensated with the tensile stresses in the mirror atoms to the SF.

It is observed that the Y_{MD} of SF-free nanorord is in good agreement with the Y_{exp} of 85 °C grown ZnO nanorods. It is estimated that the presence of a single basal plane SF is sufficient to initiate a phase transformation in the ZnO nanorod and reduces the σ_y of the ZnO nanorod. It also changes the stiffness of ZnO nanorods. Change of stiffness initiates different force distribution for different structures. This changes the maximum force withstanding capability (i.e., F_{cr}) of ZnO nanorods. Thus, an attempt of obtaining elastic modulus using analytical buckling models (while considering this changing F_{cr}) gives different elastic modulus for different structures of the same ZnO material.[19−23,35] As this elastic modulus is extensive property dependent, it does not reflect the true elastic modulus of ZnO. Here, change in stiffness of the ZnO nanorod decreases load sustainability of the structure and undergoes buckling at low applied force. Although, under HRTEM we observed a single SF, but it is also feasible that the ZnO nanorod can have more than one SF (which are sometimes destructively interfered with the e-beam due to certain zone axis oriented view) as we observed detectable presence of zinc-blende peak in XRD measurements.[36] Multiple SFs can also result in a low critical force. The methodology used in this investigation to study the mechanical properties of ZnO nanorods consists of drift correction, localization of nanorods, AFM-based compression, and fitting the FD curve with Sneddon model considering the geometry of the AFM tip. This enables us to extract the elastic modulus, which has excellent agreement with our theoretical study. However, the method is limited if there is buckling in the nanostructure at low force range and thereby does not produce enough data-points to fit a reliable curve to obtain the elastic modulus. As we see from Figure S11 that fitting a curve in the prebuckling region gives an unreliable elastic modulus of ~6 GPa. The postbuckling region (where one cannot obtain an elastic modulus) gives elastic modulus of ~8 GPa. In our case, a single nanorod can have more than one stacking fault, which can significantly reduce the strength of the nanorod compared to our theoretically predicted structure where we considered a single stacking fault. In that case, the structure undergoes buckling at a very low force range, which prevents the nanorod to reach the FD slope corresponding to the theoretically predicted elastic modulus. To date, several studies reported the nanomechanical behavior of low-dimensional materials with significant improvement in strength compared to their bulk counterparts, but rarely any study has considered the role of defects on the mechanical properties of nanocrystals. Our current study shows that structural defects play a key role in determining the yield strength of nanocrystals and enables us to

DOI: 10.1021/acs.nanolett.6b00571
Nano Lett. XXXX, XXX, XXX−XXX

interpret the mechanics of other II−VI wurtzite nanocrystals/nanorods with similar types of SFs.[37]

In summary, using AFM, HRTEM, and MD simulations we have investigated the effect of I_1-type SFs induced mechanics in wurtzite ZnO nanorods. We found that ZnO nanorods with extended I_1-type SF show buckling behavior at low critical forces. However, the SF free ZnO nanorods behave linearly in the same range. From a size-dependent study we revealed not only a size-dependent mechanical behavior (i.e., elastic modulus and yield strength) at low dimensions but also a new phase transformation kinetics showing phase transformation from WZ to HX in the presence of the I_1 SF. This changes stiffness of the ZnO nanorods and influences their AFM measured mechanical behavior. We conclude that, for electromechanical device development using nanocrystal as active material, defects play a significant role for nanomaterial failure and unexpected nonlinearity.

■ ASSOCIATED CONTENT

Supporting Information

The Supporting Information is available free of charge on the ACS Publications website at DOI: 10.1021/acs.nanolett.6b00571.

Morphology of ZnO nanorods grown at 85 °C and their cross-sectional view, interaction of a nanorod with an AFM tip, calibration of the AFM tip, Sneddon fit of FD curve, vertical nanorod selection and AFM tip interaction with the neighboring nanorods, analytical modeling of a single ZnO nanorod, modified J. B. Johnson formula for inclined column, HRTEM electron diffractogram, zinc-blende stacking, MD simulations, limitation of extracting elastic modulus from FD curve (PDF)

■ AUTHOR INFORMATION

Corresponding Authors

*(M.G.) E-mail: ghoshiisc@gmail.com.
*(S.G.) E-mail: sghosh@physik3.gwdg.de.
*(K.M.) E-mail: kzm5606@psu.edu; kmomeni@latech.edu.

Author Contributions

M.G. and S.G. contributed equally to this work.

Notes

The authors declare no competing financial interest.

■ ACKNOWLEDGMENTS

M.G is highly thankful to the Ministry of Human Resource Development, Government of India, for providing doctoral scholarship. The authors acknowledge Centre for Nano Science and Engineering, Indian Institute of Science, Bangalore and Faculty of Physics, Georg August Universität Göttingen for all experimental facilities. K.M. would like to thank Dr. A. Soghrati and Dr. B. Shiari. Computation resources provided by the National Nanotechnology Infrastructure Network Computation (NNIN/C) project at Michigan which is supported by the National Science Foundation under grant no. ECS-0335765 are gratefully acknowledged.

■ REFERENCES

(1) Fan, F. R.; Tang, W.; Wang, Z. L. *Adv. Mater.* **2016**, *28*, 1.
(2) Marino, A.; Arai, S.; Hou, Y.; Sinibaldi, E.; Pellegrino, M.; Chang, Y. T.; Mazzolai, B.; Mattoli, V.; Suzuki, M.; Ciofani, G. *ACS Nano* **2015**, *9*, 7678.
(3) Tian, Z. R.; Voigt, J. A.; Liu, J.; Mckenzie, B.; Mcdermott, M. J.; Rodriguez, M. A.; Konishi, H.; Xu, H. *Nat. Mater.* **2003**, *2*, 821.
(4) Hsu, C. L.; Chen, K. C. *J. Phys. Chem. C* **2012**, *116*, 9351.
(5) Velazquez, B. J. M.; Baskaran, S.; Gaikwad, A. V.; Ngo-Duc, T. T.; He, X.; Oye, M. M.; Meyyappan, M.; Rout, T. K.; Fu, J. Y.; Banerjee, S. *ACS Appl. Mater. Interfaces* **2013**, *5*, 10650.
(6) Lauritsen, J. V.; Porsgaard, S.; Rasmussen, M. K.; Jensen, M. C.; Bechstein, R.; Meinander, K.; Clausen, B. S.; Helveg, S.; Wahl, R.; Kresse, G. *ACS Nano* **2011**, *5*, 5987.
(7) Yang, P.; Yan, H.; Mao, S.; Russo, R.; Johnson, J.; Saykally, R.; Morris, N.; Pham, J.; He, R.; Choi, H. J. *Adv. Funct. Mater.* **2002**, *5*, 323.
(8) Dal Corso, A.; Posternak, M.; Resta, R.; Baldereschi, A. *Phys. Rev. B: Condens. Matter Mater. Phys.* **1994**, *50*, 10715.
(9) Momeni, K.; Attariani, H. *Phys. Chem. Chem. Phys.* **2014**, *16*, 4522.
(10) Momeni, K.; Attariani, H.; LeSar, R. A. *Phys. Chem. Chem. Phys.* **2016**, *18*, 19873.
(11) Asthana, A.; Momeni, K.; Prasad, A.; Yap, Y. K.; Yassar, R. S. *Nanotechnology* **2011**, *22*, 265712.
(12) Agrawal, R.; Peng, B.; Gdoutos, E. E.; Espinosa, H. D. *Nano Lett.* **2008**, *8*, 3668.
(13) Wen, B.; Sader, J. E.; Boland, J. J. *Phys. Rev. Lett.* **2008**, *101*, 175502.
(14) Momeni, K.; Asthana, A.; Prasad, A.; Yap, Y.; Yassar, R. S. *Appl. Phys. A: Mater. Sci. Process.* **2012**, *109*, 95.
(15) Ghosh, M.; Rao, M. G. *Mater. Express* **2013**, *3*, 319.
(16) Zhao, M. H.; Wang, Z. L.; Mao, S. X. *Nano Lett.* **2004**, *4*, 587.
(17) Wang, Z. L. *Science* **2006**, *312*, 242.
(18) Wang, Z. L. *Adv. Funct. Mater.* **2008**, *18*, 3553.
(19) Ahmad, M.; Zhu, J. *J. Mater. Chem.* **2011**, *21*, 599.
(20) Soomro, M. Y.; Hussain, I.; Bano, N.; Broitman, E.; Nur, O.; Willander, M. *Nanoscale Res. Lett.* **2012**, *7*, 146.
(21) Riaz, M.; Fulati, A.; Zhao, Q. X.; Nur, O.; Willander, M.; Klason, P. *Nanotechnology* **2008**, *19*, 415708.
(22) Khaderbad, M. A.; Choi, Y.; Hiralal, P.; Aziz, A.; Wang, N.; Durkan, C.; Thiruvenkatanathan, P.; Amaratunga, G. A.; Rao, V. R.; Seshia, A. A. *Nanotechnology* **2012**, *23*, 025501.
(23) Wang, X.; Song, J.; Wang, Z. L. *J. Mater. Chem.* **2007**, *17*, 711.
(24) Chen, C. Q.; Shi, Y.; Zhang, Y. S.; Zhu, J.; Yan, Y. J. *Phys. Rev. Lett.* **2006**, *96*, 075505.
(25) Yao, H.; Yun, G.; Bai, N. *J. Phys. D: Appl. Phys.* **2012**, *45*, 285304.
(26) Dai, L.; Cheong, W. C. D.; Sow, C. H.; Lim, C. T.; Tan, V. B. C. *Langmuir* **2010**, *26*, 1165.
(27) Asthana, A.; Momeni, K.; Prasad, A.; Yap, Y. K.; Yassar, R. S. *Appl. Phys. Lett.* **2009**, *95*, 172106.
(28) Sen, B.; Stroscio, M.; Dutta, M. *J. Appl. Phys.* **2011**, *110*, 024506.
(29) Bhushan, B.; Lee, H. *Faraday Discuss.* **2012**, *156*, 235.
(30) Lähnemann, J.; Jahn, U.; Brandt, O.; Flissikowski, T.; Dogan, P.; Grahn, H. T. *J. Phys. D: Appl. Phys.* **2014**, *47*, 423001.
(31) Ghosh, S.; Ghosh, M.; Seibt, M.; Rao, G. M. *Nanoscale* **2016**, *8*, 2632.
(32) Li, C.; Guo, W.; Kong, Y.; Gao, H. *Appl. Phys. Lett.* **2007**, *90*, 033108.
(33) Setoodeh, A. R.; Attariani, H.; Khosrownejad, M. *Comput. Mater. Sci.* **2008**, *44*, 378.
(34) Harrison, W. A. Electronic structure and the properties of solids. In *The Physics of the Chemical Bond*; Dover Publications: San Francisco, CA, 1989.
(35) Ni, H.; Li, X. *Nanotechnology* **2006**, *17*, 3591.
(36) Ghosh, M.; Ghosh, S.; Seibt, M.; Rao, K. Y.; Peretzki, P.; Rao, G. M. *CrystEngComm* **2016**, *18*, 622.
(37) Hughes, S. M.; Alivisatos, A. P. *Nano Lett.* **2012**, *13*, 106.

DOI: 10.1021/acs.nanolett.6b00571
Nano Lett. XXXX, XXX, XXX−XXX